Electronic Supplementary Material (ESI) for Journal of Materials Chemistry A.
This journal is © The Royal Society of Chemistry 2024

# Electronic Supplementary Information

## Intrinsic bimetallic cations regulating band center and reactive sites boosting $CO_2$ photoreduction

Jingjing Wang[1,2], Fang Chen[1], Qing Liu[3], Hongwei Huang*[,1]

## Methods

**1. Samples preparation.** All of the reagents used in this work were analytical grade and used as received without further purification. The water used throughout the experiment was ultrapure water.

CBOB-c1 nanosheets were synthesized through a one pot hydrothermal method as follows: 1 mmol $Bi(NO_3)_3•5H_2O$ and 1 mmol $Cd(CH_3COO)_2•2H_2O$ were dissolved in 15 ml of ultrapure water, stirred for 0.5 h, and then slowly mixed with 15 ml of KBr solution (0.067 mol/L). After vigorously stirring the mixed solution to form a uniform solution, $NH_3•H_2O$ was added dropwise until the pH of the solution was adjusted to 10. After thoroughly stirring, the above mixed liquid was transferred to a Teflon-lined autoclave (50 mL) and heated at 180 ℃ for 12 hours. The light yellow products were obtained by centrifugation after natural cooling, washed three times with ethanol and water respectively, and dried at 60℃ in an air drying oven for 10 h. The preparation process of CBOB-c2 and CBOB-c3 was the same as the above route, except that the addition amount of $Cd(CH_3COO)_2•2H_2O$ was changed to 3 mmol and 5 mmol, respectively. The synthesis method of BOB and BOB/CBOB composites was similar to that of CBOB-c1, except that the pH of the precursor mixed solution was adjusted to 8 and 9, respectively.

**2. Samples characterizations.**

The crystal structure and phase information of the as-synthesized samples were determined by X-ray powder diffraction (XRD, D8-Advance (Bruker) automated X-ray diffractometer system). The microstructure and morphology of the sample were observed by field emission scanning electron microscopy (FESEM, JEOL S-4800, Hitachi, Japan). Transmission electron microscopy was applied to investigate the crystallinity and exposed crystal planes of materials (TEM, JEM-2100, JEOL, Japan). Atomic force Microscope (AFM) was equipped with Bruker Dimension Icon (Bruker Dimension Icon, GER) for use. The X-ray photoelectron spectroscopy (XPS) was conducted on the ESCALAB 250Xi instrument (Thermp Fisher, UK). The content of metal elements in each sample was quantitatively analyzed by inductively coupled plasma emission spectrometer (ICP-OES 725, Agilent, USA). UV-vis diffuse

reflectance spectroscopy (DRS) was implemented on the UV-VIS spectrophotometer (U-3900, Hitachi, Japan) using white $BaSO_4$ as a reference. The Raman spectrometer (LabRAM HR Evolution, France) was carried out to identify the material composition of the sample. The wettability of the sample to $H_2O$ was examined by the Contact angle meter (CA, JC2000D, China) adopting the five point fitting analysis method, where the powder sample was compressed into a dense circular plate under high pressure. Photoluminescence (PL) spectroscopy (Hitachi, F-4600, Japan, 150W Xe lamp) was applied to detect the relative intensity of charge recombination between as-prepared samples. The fluorescence lifetime of photocatalysts was ascertained by the resolved fluorescence emission spectrum obtained from a fluorescence spectrophotometer (Edinburgh Instruments, FLS1000). The specific surface area and $CO_2$ uptake were quantitatively measured by a fully automated physical adsorption instrument in $N_2$ and $CO_2$ atmospheres, respectively. $CO_2$-Temperature programmed desorption (TPD) was operated on the Micromeritics Auto chem II 2920 analyzer.

**3. In situ FT-IR measurement**

The intermediate species and predicted possible pathways for photocatalytic conversion of $CO_2$ and $H_2O$ were analyzed by in situ Fourier transform infrared spectroscopy (FT-IR) obtained from a Bruker Vertex 70v spectrometer. Specifically, the photocatalyst was coated on ATR crystals and subjected to vacuum treatment for 30 minutes. Secondly, high-purity $CO_2$ and $H_2O$ vapors were transported into the gas pipeline and maintained at an atmospheric pressure, and the system reached an adsorption equilibrium state of $CO_2$ and $H_2O$ in the dark state for 30 minutes. Finally, the photocatalyst was illuminated by simulated sunlight for 30 minutes. A series of IR spectra waere repeatedly collected every 2 minutes at the same time.

**4. Photoelectrochemical tests.**

The transient photocurrent response, Mot-Schottky plots, and electrochemical impedance spectrum (EIS) tests of the as-synthesized samples were performed on the electrochemical workstation (CHI-660E, Chenhua Instrument Co., Ltd). Among them, the three-electrode system was employed involving a saturated calomel electrode (SCE) as the reference electrode, Pt wire as the counter electrode, and indium-tin-oxide (ITO)

glasses coated with the as-synthesized sample as the working electrode. 0.1M $Na_2SO_4$ solution acts as the electrolyte solution for this three-electrode-system. Specifically, 10 mg of photocatalyst was dispersed in 1ml of ethanol solution containing ethyl cellulose (1mg/mL) after ultrasound for 30 minutes. Subsequently, this uniform slurry was slowly dropped onto the ITO substrate and naturally dried, and finally dried at 60 ℃ for 4 h to obtain the final sample. During the measuring process, a xenon lamp (300 W) was employed as the light source for illuminating the sample at room temperature with a sample range of 30 mm × 25 mm.

**5. Photocatalytic $CO_2$ reduction test.**

A series of photocatalytic $CO_2$ reduction activity tests of as-prepared photocatalysts were carried out in a liquid-solid gas three-phase reactor, and the gas products were obtained from a PLS-SXE300 Labsolar-IIIAG closed circulation system (Perfectlight, China). Specifically, 20 mg of the synthesized sample and 30 mL of ultrapure water were added to the reactor and uniformly dispersed by ultrasound for 5 minutes. Then, the reactor was treated by vacuum for 10 minutes to remove air from the system and blown with high-purity $CO_2$ gas to 1 atmospheric pressure. The constant stirring before illumination aimed to increase the solubility of $CO_2$ in water and catalyst surfaces and maintain adsorption-desorption equilibrium. Finally, a 30W xenon lamp (Perfectlight, China) was employed as a light source to illuminate the reaction system from above the reactor and maintain the reactor temperature at 298K. Every hour, 1ml of the reaction gas was extracted from the reactor using a syringe and quantitatively analyzed by GC9790II gas chromatograph (Zhejiang Fuli Analytical Instrument Co., Ltd., China). Similar to the above conditions, the three control experiments were only conducted without turning on the xenon lamp, in Ar atmosphere without $CO_2$, and without photocatalyst, respectively. $^{13}CO_2$ (Beijing Gaisi Chemical Gases Company) was used for carbon source tracking detection.

**6. Density functional theory (DFT) calculations.**

Density Functional Theory (DFT) calculations were executed to accomplish structure relaxation, electron band structure, DOS, and single point energy evaluation initiated by the Vienna Ab initio Simulation Package (VASP) code. The Perdew-Burke-

Ernzerhof (PBE) of functional of generalized gradient approximation (GGA) was utilized to investigate the exchange-correlation of valence electrons. The lattice parameters of the target crystal were determined by setting the plane wave cut-off energy to 450 eV, the k-point density of 4×4×1 in the Brillouin zone of the unit cell, the self-consistent-field energy convergence threshold of $10^{-5}$, and the convergence of force of -0.03 eV $Å^{-1}$. All the computational parameters were set as fine to verify the accuracy of the present purpose. The adsorption energy of $CO_2$ molecules was defined by the following equation: $E_{ads} = E_{tot} - (E_{mol} + E_{CBOB})$, where $E_{tot}$, $E_{mol}$ and $E_{CBOB}$ refer to the total energy of the adsorption composite structure, the isolated adsorbed molecule and the free CBOB structure, respectively.

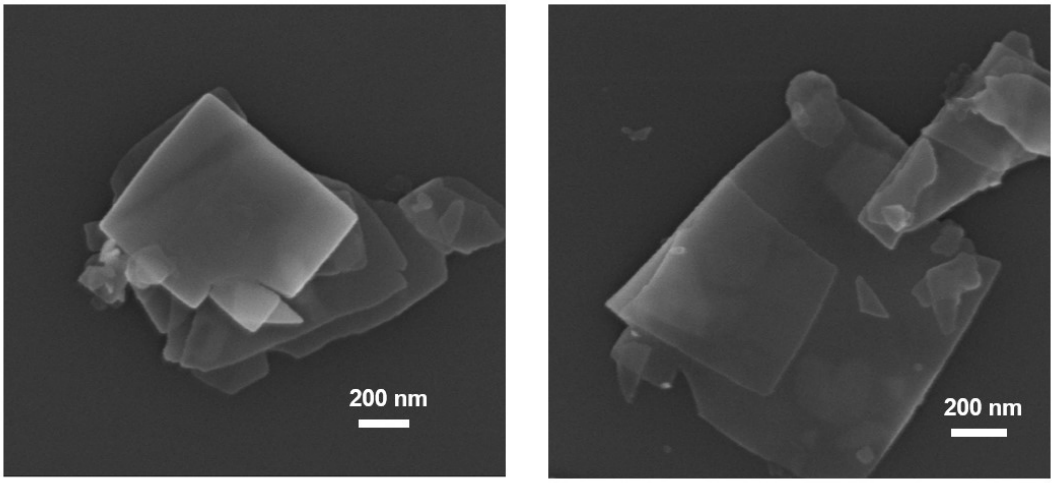


**Figure S1.** SEM images of CBOB-c1 sample.

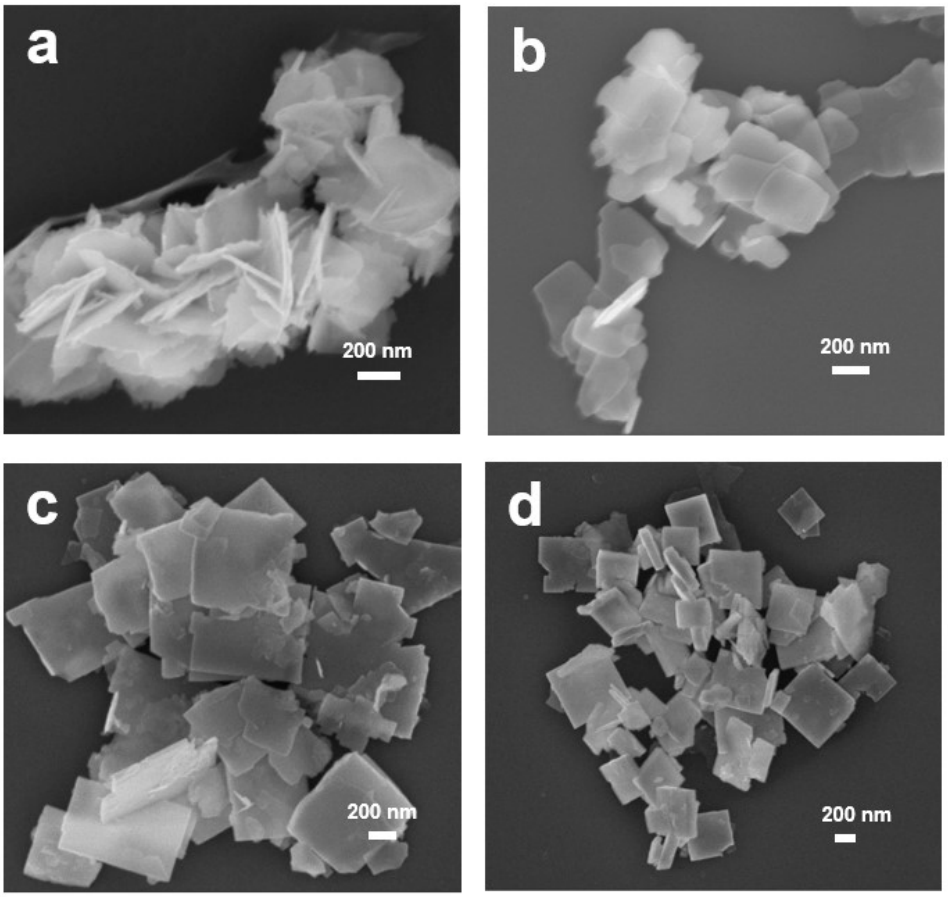


**Figure S2.** SEM images of BOB (a), BOB/CBOB (b), CBOB-c2 (c) and CBOB-c3 (d) samples .

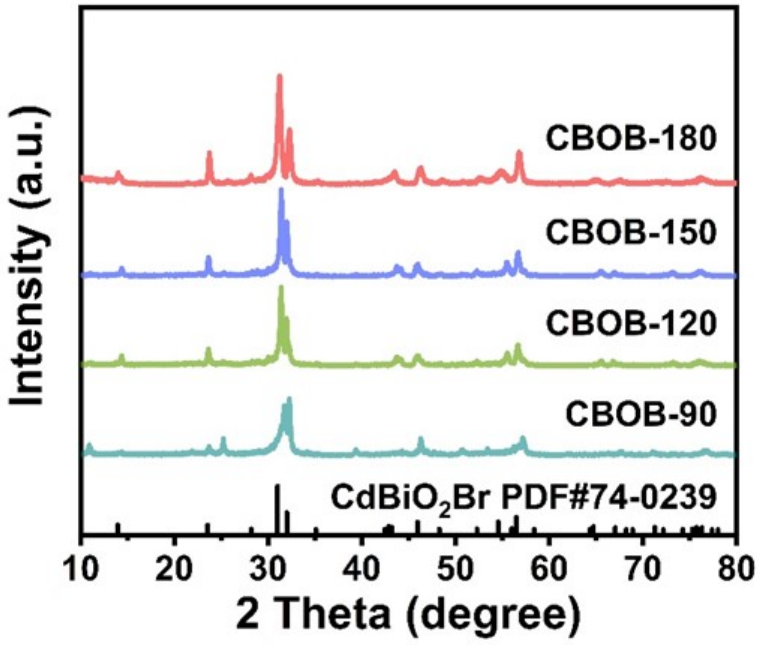


**Figure S3.** The XRD patterns of CBOB-90, CBOB-120, CBOB-150 and CBOB-180.

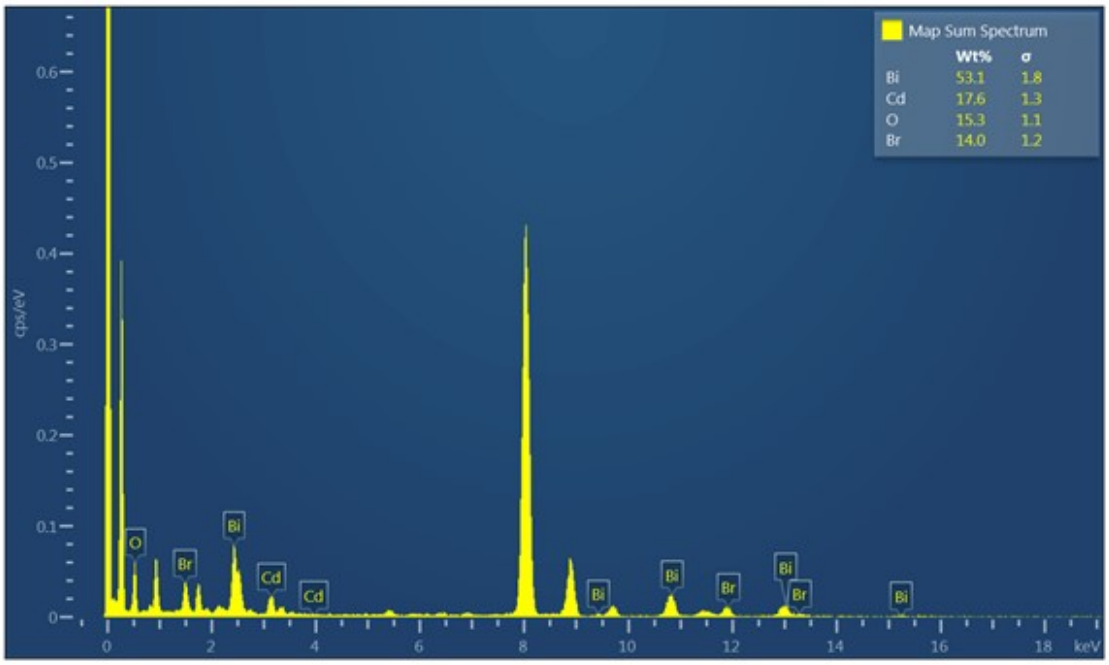


**Figure S4.** EDS element analysis of CBOB-c1.

**Table S1.** The molar ratio of Cd and Bi in BOB/CBOB, CBOB-c1 and CBOB-c2 samples measured by ICP test results.

| Molar ratio | BOB/CBOB | CBOB-c1 | CBOB-c2 |
|---|---|---|---|
| Bi | 0.76 | 0.75 | 0.67 |
| Cd | 0.24 | 0.25 | 0.33 |

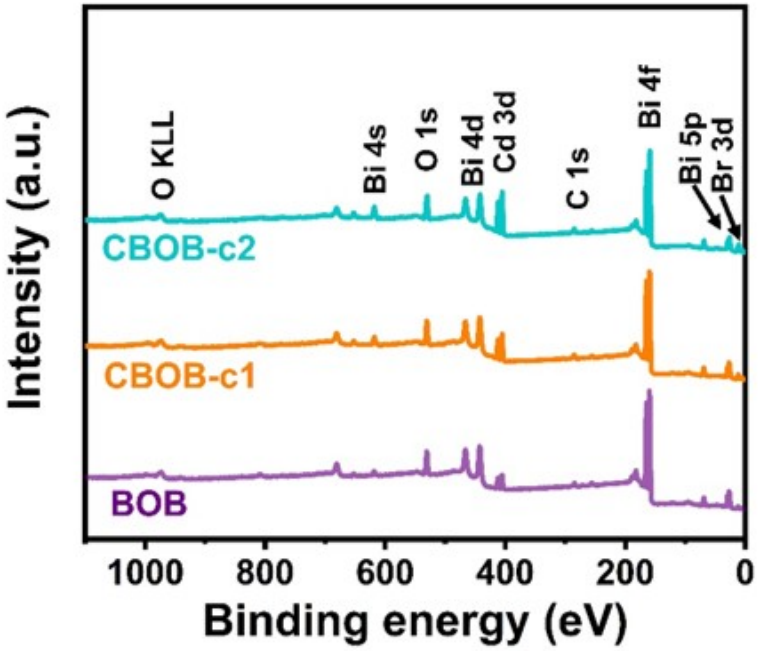


**Figure S5.** The XPS survey spectra of BOB, CBOB-c1 and CBOB-c2 samples.

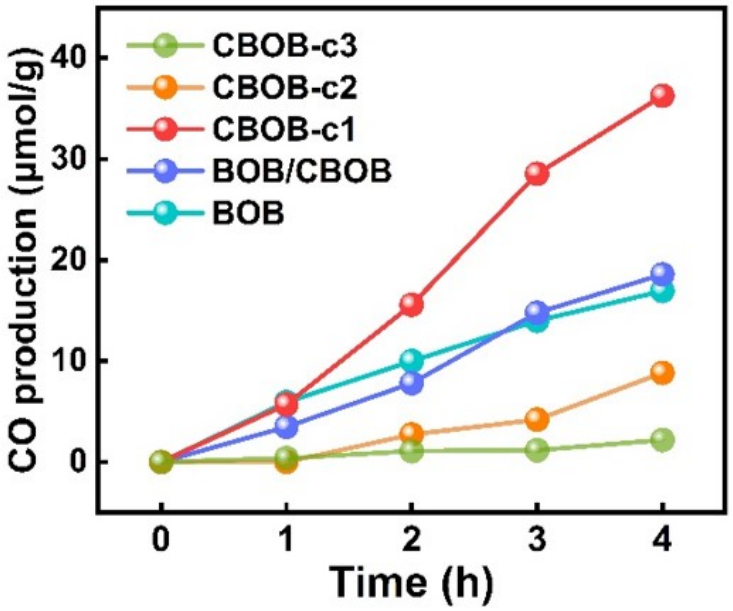


**Figure S6.** CO production cures of BOB, BOB/CBOB, CBOB-c1, CBOB-c2 and CBOB-c3 under simulated solar light.

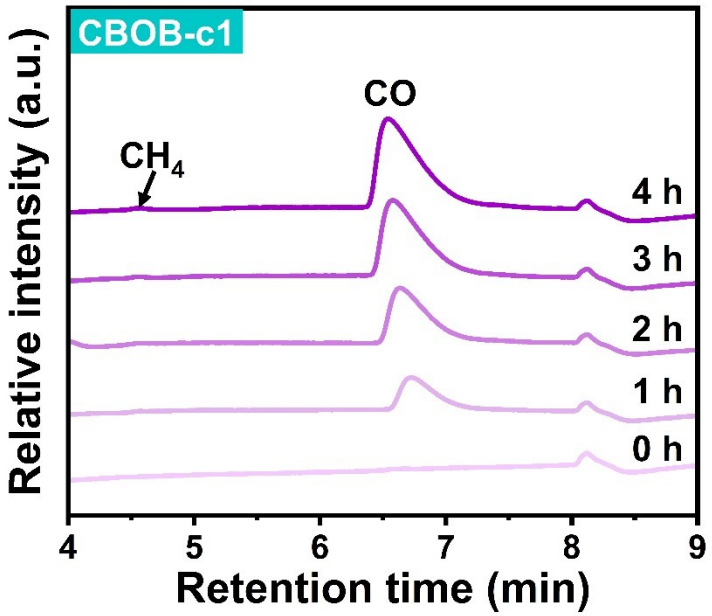


**Figure S7.** Gas chromatograms of CBOB-c1 under simulated solar light.

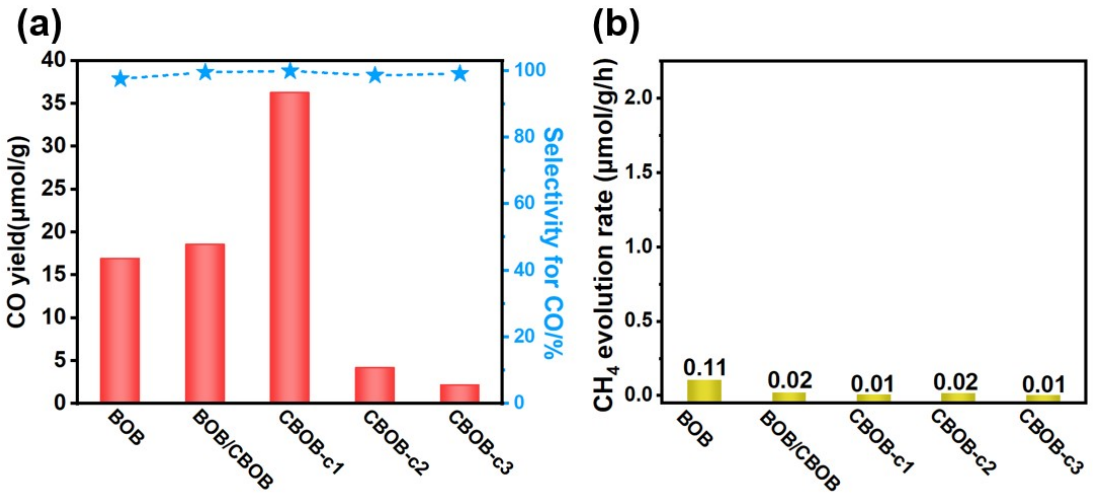


**Figure S8.** (a)The CO yield and selectivity for CO; (b)The production rates of $CH_4$ generated in the $CO_2$ reduction process over BOB, BOB/CBOB, CBOB-c1, CBOB-c2 and CBOB-c3.

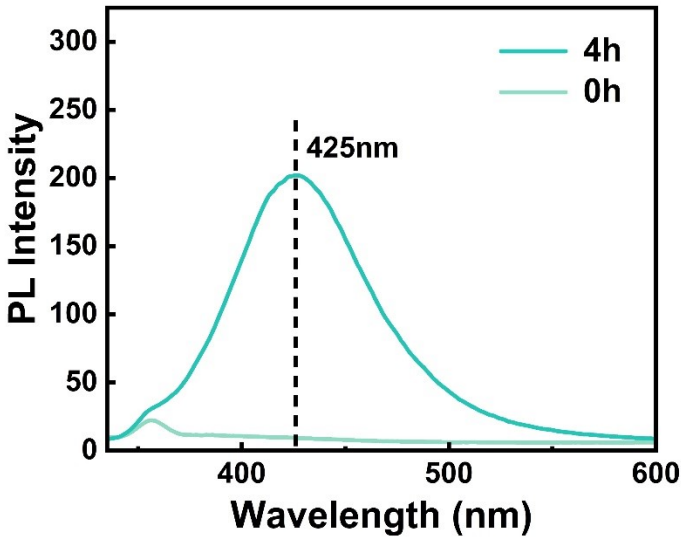


**Figure S9.** Fluorescence spectra of TA solution over CBOB-c1 under light irradiation.

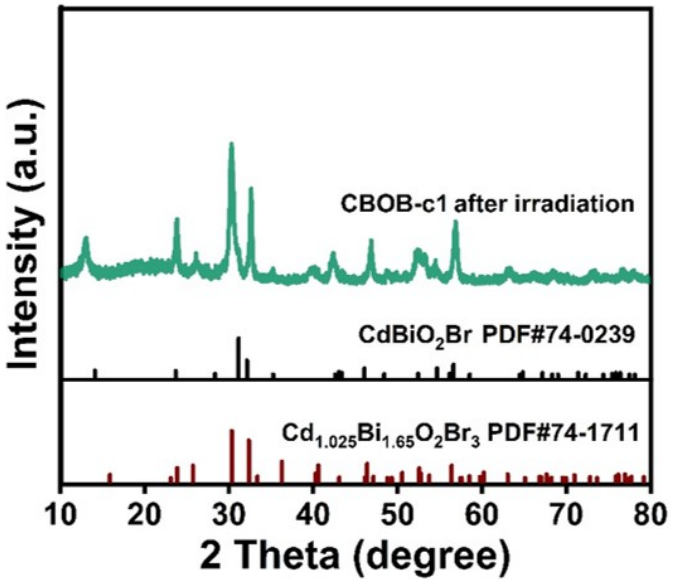


**Figure S10.** XRD patterns of CBOB-c1 after 4h photocatalytic $CO_2$ reduction reaction.

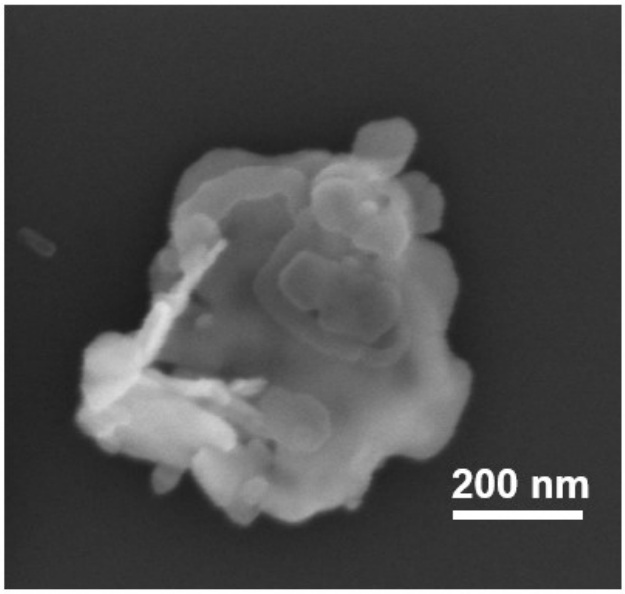


**Figure S11.** SEM image of CBOB-c1 after 4h photocatalytic $CO_2$ reduction reaction.

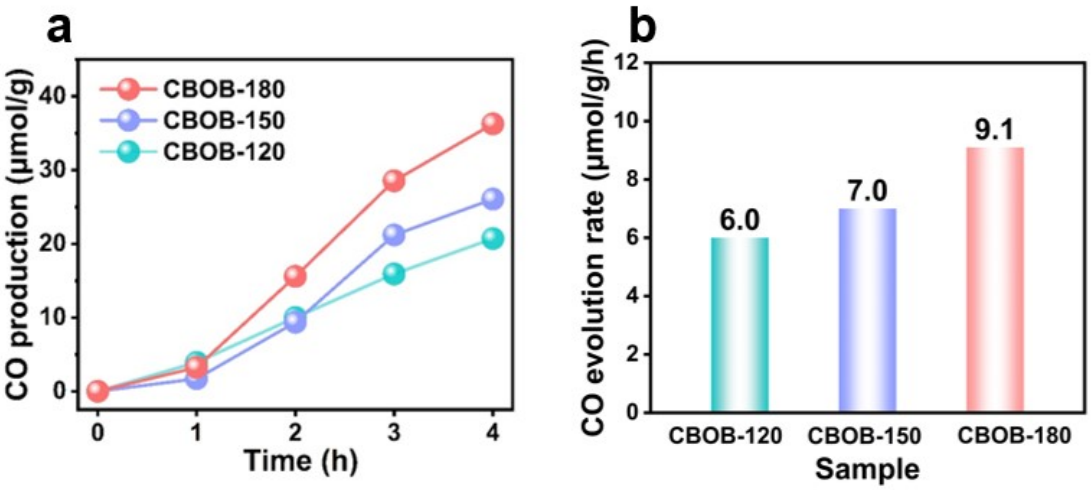


**Figure S12.** (a) CO production cures and (b) production rates of CBOB-120, CBOB-150 and CBOB-180(CBOB-c1) under simulated solar light.

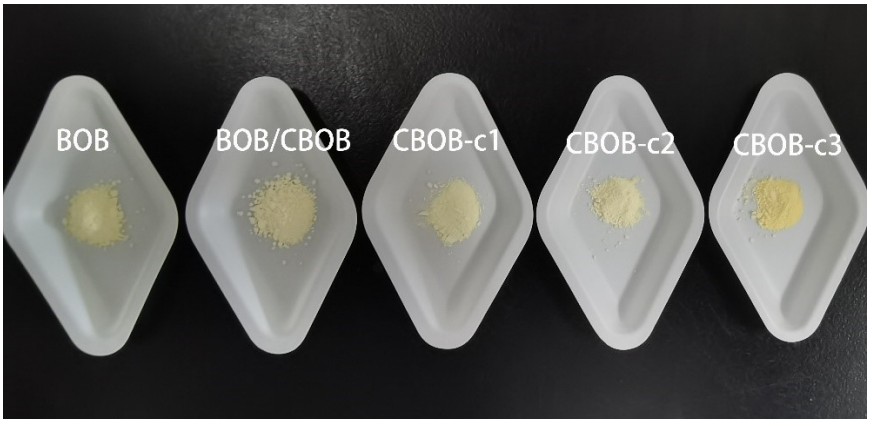


**Figure S13.** Pictures of BOB, BOB/CBOB, CBOB-cl, CBOB-c2 and CBOB-c3.

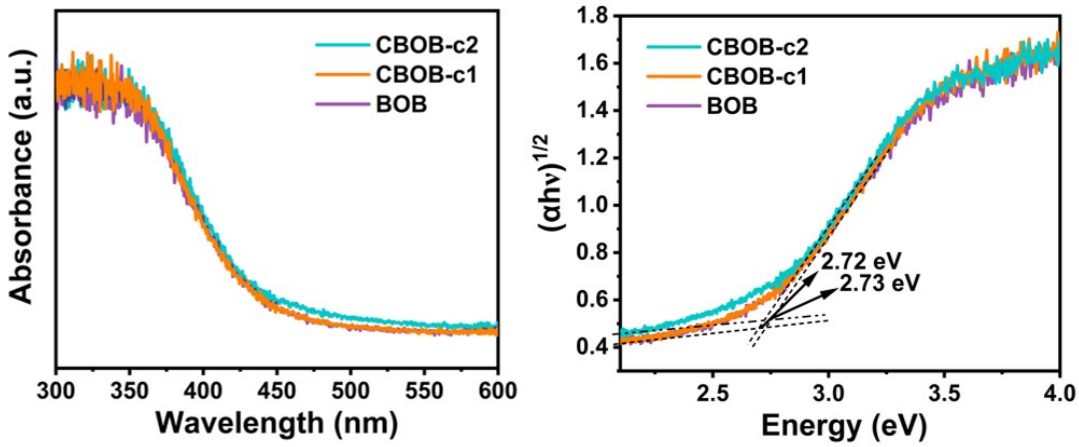


**Figure S14.** UV-vis diffuse reflectance spectra (left), plots of the transformed Kubelka-Munk function for as-prepared BOB, CBOB-c1 and CBOB-c2 (right).

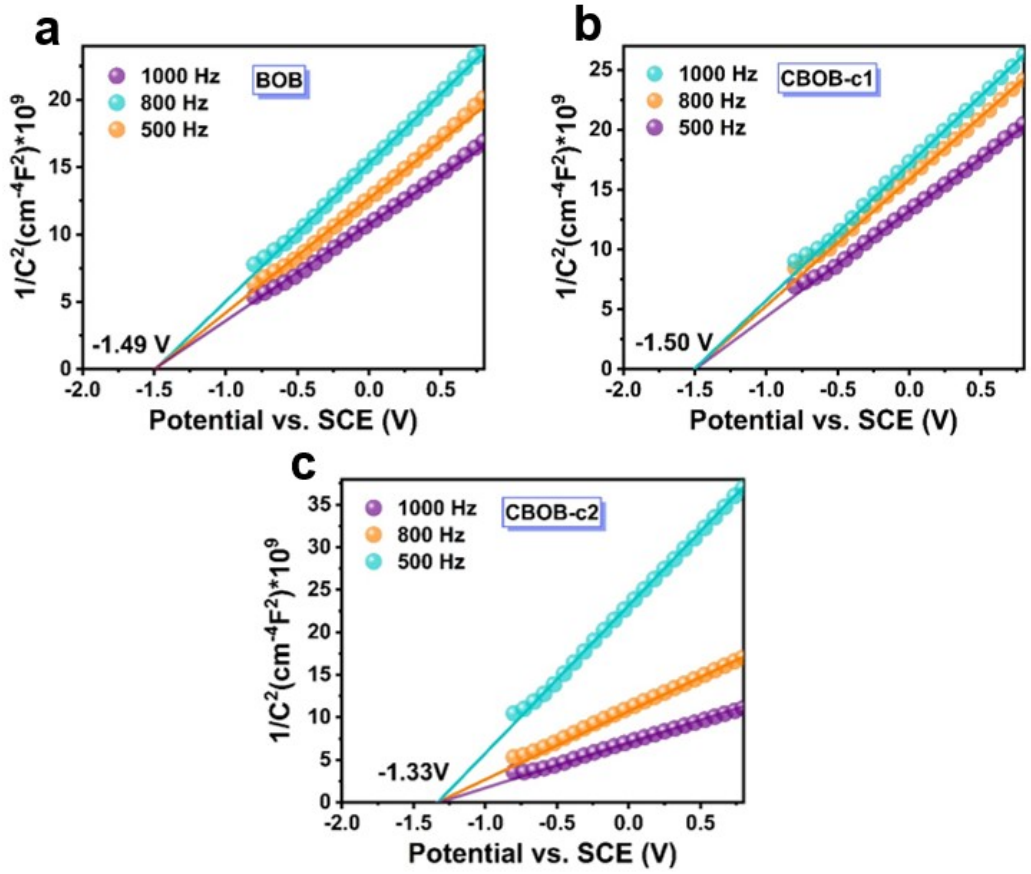


**Figure S15.** The Mott-Schottky plots of BOB (a), CBOB-c1 (b) and CBOB-c2 (c) at frequencies of 500 Hz, 800 Hz, 1000 Hz.

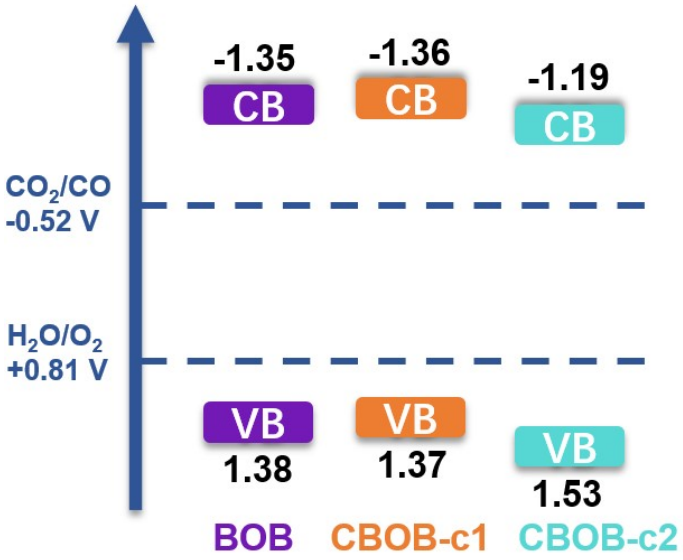


**Figure S16.** Schematic illustration for band structures of BOB, CBOB-c1 and CBOB-c2.

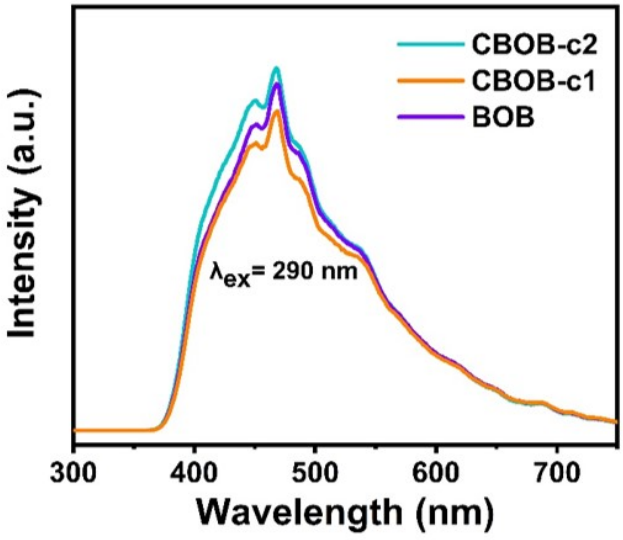


**Figure S17.** PL spectra of BOB, CBOB-c1 and CBOB-c2.

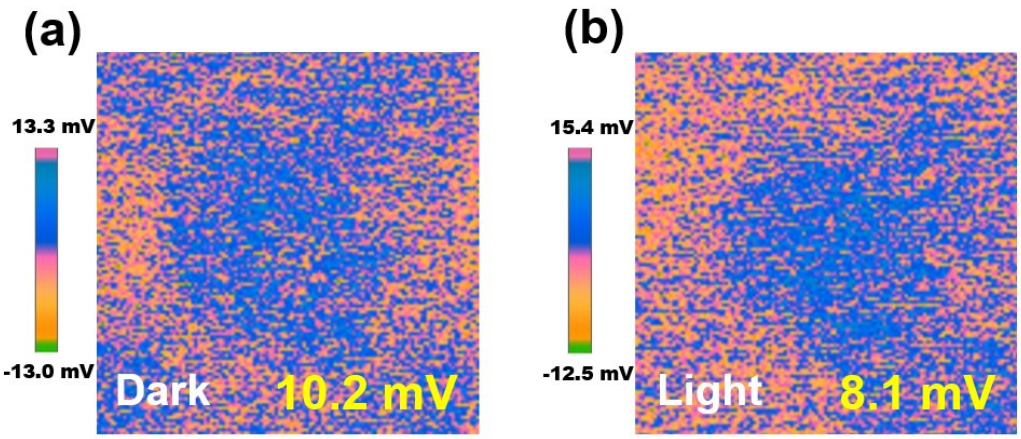


**Figure S18.** (a) 3D surface potential distributions of BOB in the dark and (b) BOB under light illumination.

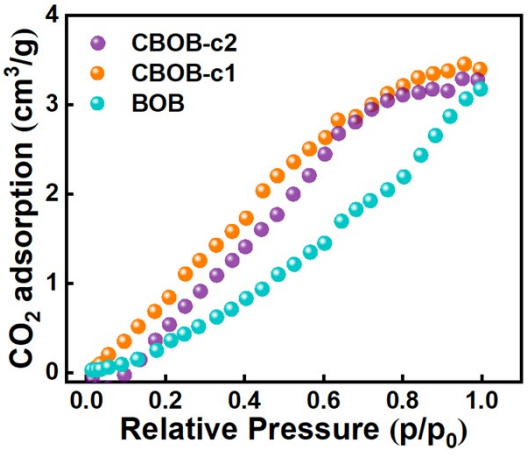


**Figure S19.** The $CO_2$ adsorption isotherms of BOB, CBOB-c1 and CBOB-c2.

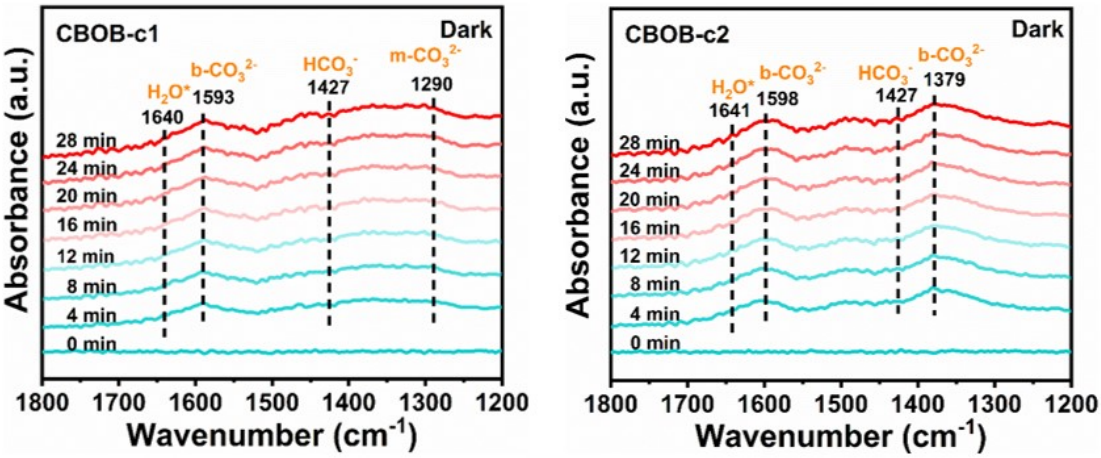


**Figure S20.** The in-situ FTIR of CBOB-c1 (left) and CBOB-c2 (right) in dark condition under $CO_2$ atmospheres with $H_2O$ vapor.

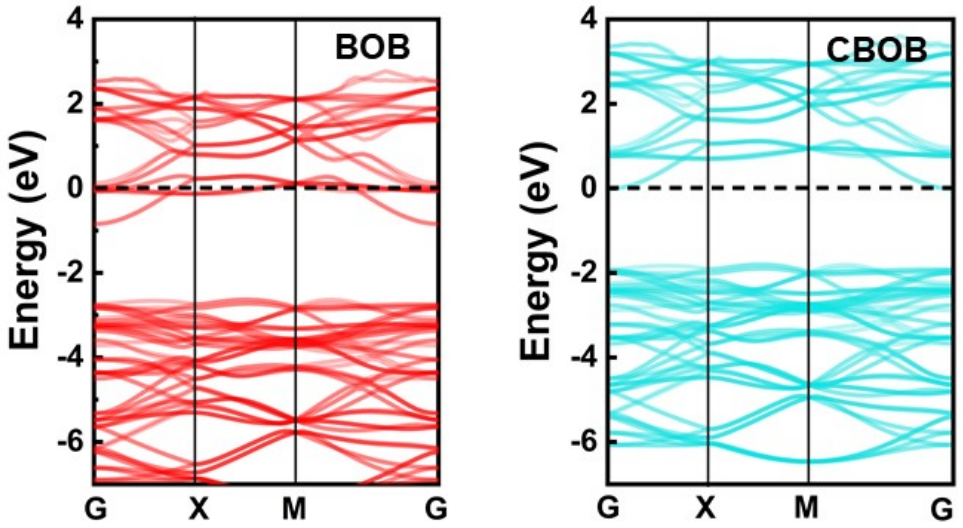


**Figure S21.** Band structures of BOB and CBOB.

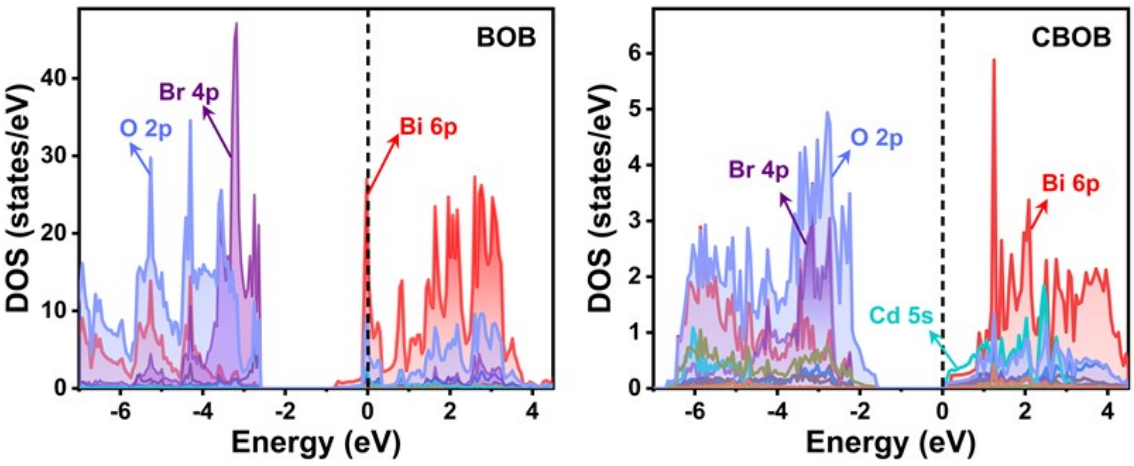


**Figure S22.** DOS diagrams of BOB (left) and CBOB (right).

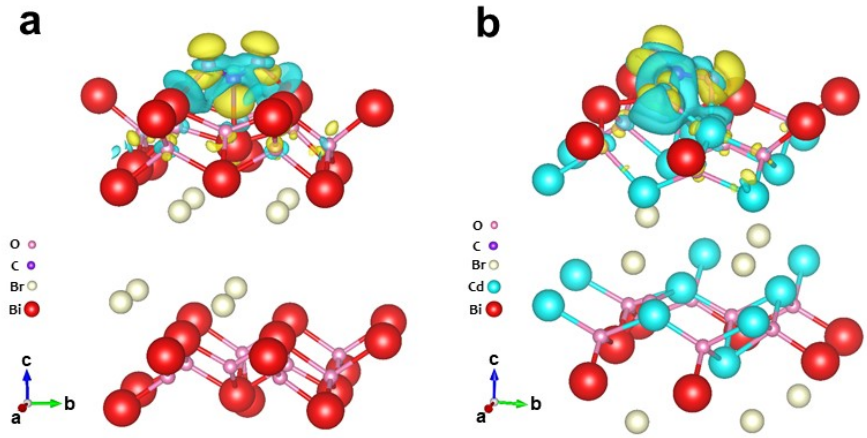


**Figure S23.** Charge difference of $CO_2$ absorbed BOB (a) and CBOB (b). Charge accumulation is in yellow and depletion is in blue.

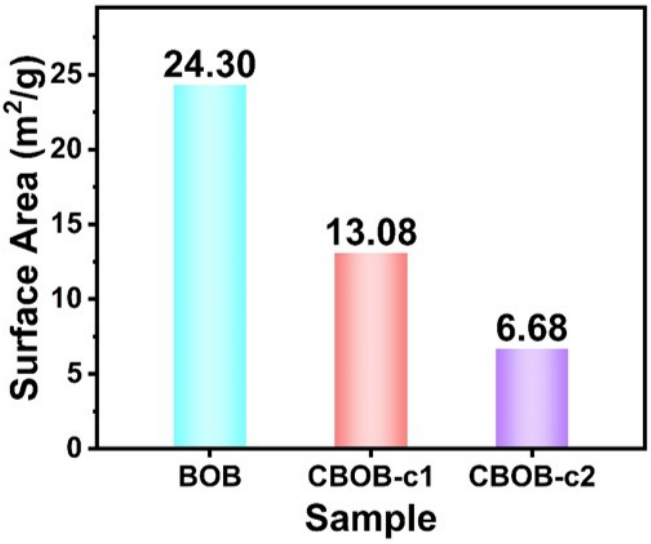


**Figure S24.** The BET specific surface areas of BOB, CBOB-c1 and CBOB-c2.

**Table S2.** Comparison of $CO_2$ photoreduction performance parameters of photocatalysts.

| Photocatalyst | Light source | Catalytic system | CO production rate (μmol/g/h) | Ref. |
|---|---|---|---|---|
| $Cd_{0.46}Bi_{1.36}O_2Br$ | 300W Xe lamp | $20mg_{cat}$+30mL $H_2O$ | 9.1 | This work |
| 0.18wt%Cu/BiOCl | 300W Xe lamp | $20mg_{cat}$+100mL $H_2O$ | 6.38 | [a1] |
| 14mol%$Bi_2Al_4O_7$/β-$Bi_2O_3$ | 300W Xe lamp | $50mg_{cat}$+5mL $H_2O$ | 1.32 | [a2] |
| CoOx/$ZnFe_2O_4$ | 300W Xe lamp+AM1.5 filter | $10mg_{cat}$+0.5mL $H_2O$ | 4.56 | [a3] |
| defective $Bi_2MoO_6$ | 300W Xe lamp | $30mg_{cat}$+50mL $H_2O$ | 3.62 | [a4] |
| CdS/$CdWO_4$ | 300W Xe lamp | $20mg_{cat}$+ $H_2O$ vapor | 4.16 | [a5] |
| 20 wt%$Bi_2S_3$ QDs/g-$C_3N_4$ | 300W Xe lamp | $50mg_{cat}$+100mL $H_2O$ | 6.84 | [a6] |
| BiOBr | 300W Xe lamp | $50mg_{cat}$+ $H_2O$ vapor | 4.45 | [a7] |
| surface-Ti-rich $SrTiO_3$ | 300W Xe lamp | $20mg_{cat}$+10μL $H_2O$ | 3.07 | [a8] |
| ZnO | 300W Xe lamp | $150mg_{cat}$+ $H_2O$ vapor | 3.81 | [a9] |
| $BiOIO_3$ | 300W Xe lamp | $50mg_{cat}$+ $H_2O$ vapor | 5.42 | [a10] |
| Surface halogenation $Bi_2O_2(OH)(NO_3)$ | 300W Xe lamp | $20mg_{cat}$+ $H_2O$ vapor | 8.12 | [a11] |

**References:**


[a1] Y. Wang, H. Wang, L. Guo, T. He, J. Colloid Interface Sci. 2023, 648, 889.

[a2] Y. Liu, J. guo Guo, Y. Wang, Y. juan Hao, R. hong Liu, F. tang Li, Green Energy Environ. 2021, 6, 244.

[a3] X. Liu, Y. Chen, Q. Wang, L. Li, L. Du, G. Tian, J. Colloid Interface Sci. 2021, 599, 1-11.

[a4] J. Di, X. Zhao, C. Lian, M. Ji, J. Xia, J. Xiong, W. Zhou, X. Cao, Y. She, H. Liu, K. P. Loh, S. J. Pennycook, H. Li, Z. Liu, Nano Energy. 2019, 61, 54.

[a5] Y. Y. Li, Z. H. Wei, J. Bin Fan, Z. J. Li, H. C. Yao, Appl. Surf. Sci. 2019, 483, 442.

[a6] R. Guo, X. Liu, H. Qin, Z. Wang, X. Shi, W. Pan, Z. Fu, J. Tang, P. Jia, Y. Miao, J. Gu, Appl. Surf. Sci. 2020, 500, 144059.

[a7] D. Wu, L. Ye, H. Y. Yip, P. K. Wong, Catal. Sci. Technol. 2017, 7, 265.

[a8] C. Luo, J. Zhao, Y. Li, W. Zhao, Y. Zeng, C. Wang, Appl. Surf. Sci. 2018, 447, 627.

[a9] X. Liu, L. Ye, S. Liu, Y. Li, X. Ji, Sci. Rep. 2016, 6, 38474.

[a10] F. Chen, H. Huang, L. Ye, T. Zhang, Y. Zhang, X. Han, T. Ma, Adv. Funct. Mater. 2018, 28, 1804284.

[a11] L. Hao, L. Kang, H. Huang, L. Ye, K. Han, S. Yang, H. Yu, M. Batmunkh, Y. Zhang, T. Ma, Adv. Mater. 2019, 31, 1900546.